

CRACK GROWTH PREDICTIONS IN ALUMINUM AND TITANIUM ALLOYS UNDER AIRCRAFT LOAD SPECTRA

J. C. Newman, Jr.

Department of Aerospace Engineering, Mississippi State University, Mississippi State, MS, USA 39762

ABSTRACT

The present paper is concerned with some recent improvements that have been made in the crack-closure model, FASTRAN. Improvements were related to more accurate development of the plasticity-induced crack-closure mechanism, especially, for high stress ratio spectra, and to using improved fatigue-crack-growth-rate data in the threshold regime. The model was used to correlate fatigue-crack-growth rates under constant-amplitude loading for an aluminum and titanium alloy. The model was then used to predict fatigue-crack growth under simulated aircraft load spectra, such as a High Speed Civil Transport spectrum and a transport wing (gust and maneuver) spectrum. The paper will demonstrate how constraint (plane stress and plane strain) plays a leading role in retardation and acceleration effects that occur under variable-amplitude loading. Comparisons made between measured and predicted crack-length-against-cycles for the aluminum and titanium alloy under the two aircraft load spectra agreed quite well ($\pm 20\%$) with the test results.

1 INTRODUCTION

During the past 30 years, a number of load-interaction models have been developed to predict fatigue-crack growth under aircraft spectrum loading. These models have generally been based on plastic deformations that develop at the crack front, and has either been empirical or based on physical models of crack-growth and closure. Since the discovery of the plasticity-induced closure mechanism [1], several other closure or shielding mechanisms have been identified, such as roughness- [2] and oxide-induced closure. However, these other mechanisms have yet to be incorporated into any of major life prediction codes, such as NASGRO [3] or AFGROW [4].

Brot and Matias [5], Israel Aircraft Industries, made an evaluation of several load-interaction models on four aluminum alloys, two crack configurations, and five load spectra. They found that the NASA strip-yield model correlated well with the test data and had the least variation, over the range of testing, compared to other models. But their study did illustrate some deficiencies with the NASA strip-yield model, especially for high stress ratio spectra and for cracks emanating from an open hole. Research at NASA on the High-Speed Civil Transport (HSCT) aircraft has also produce spectrum data on some candidate titanium alloys using a high stress ratio spectrum [6].

The objective of this paper is to present some improvements that have been made in the crack-closure model, FASTRAN [7]. The improvements are related to more accurate development of the plasticity-induced closure mechanism, especially, for high stress ratio spectra, and to using improved fatigue-crack-growth rate data in the near threshold regime. The model was used to correlate fatigue-crack-growth-rate data under constant-amplitude loading for an aluminum and titanium alloy. The model was then used to predict crack growth under simulated aircraft load spectra, such as a High Speed Civil Transport spectrum and a transport wing (gust and maneuver) spectrum studied by Brot and Matias. The paper will demonstrate how constraint (plane stress and plane strain) plays a leading role in the retardation and acceleration effects that occur under variable-amplitude loading. Comparisons are made between measured and predicted crack-length-against-cycles for the aluminum and titanium alloys under the two aircraft load histories.

2 MATERIALS AND CRACK CONFIGURATIONS

Fatigue-crack-growth and fracture data on 7075-T7351 aluminum alloy plate ($B = 6.35$ mm) were obtained from the NASGRO materials database [3], which is data from middle-crack-tension, M(T), and compact, C(T), specimens. The yield stress (σ_{ys}) and ultimate tensile strength (σ_u) of

the aluminum alloy were 450 and 520 MPa, respectively. The M(T) specimens were 80 mm wide (2w). The open-hole specimen was identical to the M(T) specimen, except a hole of 8 mm diameter was centrally located. Each specimen had an EDM notch and was fatigue pre-cracked under constant-amplitude loading to an initial crack length. The specimens were then subjected to a wing gust and maneuver spectrum typically of transport aircraft.

Fatigue-crack-growth and fracture results on the thin-sheet Ti-62222 STA titanium alloy (B = 1.6 to 1.75 mm) were obtained from several sources. Phillips [6] conducted constant-amplitude tests on M(T) specimens (2w = 51- and 76-mm). Smith and Piascik [8] and Liknes and Stephens [9] conducted tests on eccentrically-loaded-single-edge-crack tension, ESE(T), specimens (w = 76-mm). Worden (Boeing Co.) conducted tests on M(T) specimens (2w = 254-mm). The yield stress and ultimate tensile strength were 1190 and 1310 MPa, respectively. In addition, Phillips [6] conducted spectrum fatigue-crack-growth tests on M(T) specimens using the HSCT spectrum.

3 FATIGUE-CRACK-GROWTH RATES

The crack-growth-rate relation used in FASTRAN was

$$dc/dN = C_i (\Delta K_{eff})^{n_i} / [1 - (K_{max}/K_{Ic})^q] \quad (1)$$

where C_i and n_i are the coefficient and power for each linear segment in a multi-linear rate curve, K_{max} is the maximum stress-intensity factor, K_{Ic} is the elastic stress-intensity at failure (function of crack length, width, and specimen type), and q was set to 2. Newman [10] developed the Two-Parameter Fracture Criterion (TPFC) to correlate and to predict failure loads on cracked metallic materials. Using the TPFC equation, the elastic stress-intensity factor at failure for $S_n < \sigma_{ys}$ is

$$K_{Ic} = K_F / \{1 - m K_F / [S_u \sqrt{(\pi c) F_n}]\} \quad (2)$$

where K_F and m are the two fracture parameters, S_n is the net-section stress, and S_u is the plastic-hinge stress based on the ultimate tensile strength. For example, for an M(T) specimen S_u is equal to σ_u , the ultimate tensile strength; and for a pure bend specimen, $S_u = 1.5 \sigma_u$. A similar equation was derived for $S_n > \sigma_{ys}$, see Reference 10. The m -value is both a material and configuration parameter, and is a function of material, thickness, and specimen type (tension, bending, etc.). For brittle materials, $m = 0$ and the fracture toughness K_F is equal to the elastic stress-intensity at failure (like, K_{Ic} , the plane-strain fracture toughness). However, for very ductile materials, $m = 1$ and the fracture toughness K_F is the elastic-plastic fracture toughness; and K_F is the limiting value of K_{Ic} for very large panels and at very low failure stresses. For $m = 1$ and a very large K_F value, the TPFC equation reduces to a net-section-stress-equal-ultimate-tensile-strength failure criterion. Once K_F and m are known for a material, thickness, and specimen configuration, then the K_{Ic} values can be predicted for a given crack length and specimen width. Note that F_n is the usual boundary-correction factor (F) on stress-intensity factor with a net-to-gross section conversion.

To make crack-growth predictions, ΔK_{eff} as a function of crack-growth rate must be obtained over a wide range in rates (from threshold to fracture), especially if spectrum load predictions are required. Under constant- amplitude loading, the only unknown in the crack-closure analysis is the constraint factor, α . The constraint factor was determined by finding (by trial-and-error) a value (or values) that will correlate the constant-amplitude crack-growth-rate data over a wide range in stresses ratios [11]. In the following, the ΔK_{eff} -rate relations were developed.

3.1 Aluminum alloy – 7075-T7351

The NASGRO materials database was used to obtain the fatigue-crack-growth-rate data on the aluminum alloy plate (B = 6.35 mm). The ΔK -rate data from both M(T) and C(T) specimens were

analyzed to determine the constraint factors (α) to best fit the data; and the results are shown in Figure 1. This figure shows Elber's effective-stress-intensity-factor, ΔK_{eff} , against crack-growth rate. The crack-opening stresses from the FASTRAN model were used to correlate the data. The constraint-loss regime has been associated with the transition from flat-to-slant (45°) crack growth [12]. The dashed vertical line shows the estimated value ($20 \text{ MPa}\sqrt{\text{m}}$) where the flat-to-slant crack-growth transition should occur for this material. Currently, the selection of the constraint factors and their associated rates has to be obtained by trial-and-error. It is, however, suspected that the start of the slant-crack growth regime is independent of plate thickness and occurs as the plastic zone at the free surface begins to allow shear deformations and slant crack growth. But the attainment of the fully slant-crack growth (45°) is a function of the plate thickness. For crack-growth rates less than $8\text{e-}7 \text{ m/cycle}$, a constraint factor, α , of 1.8 was used; but above a rate of $8\text{e-}5 \text{ m/cycle}$, a constraint factor, α , of 1.2 (like plane stress) was used. The crack-closure model correlated the fatigue-crack-growth rate data in a tight band. More scatter or variations were observed in the constraint-loss regime and in the near threshold regime. In the constraint-loss regime, the small width specimens ($w = 51 \text{ mm}$) at the higher R ratios were approaching the fracture toughness of the material. In the threshold regime, the results on the compact specimens were determined by using a load-reduction procedure. It has been shown that the load-reduction procedure may induce higher thresholds due to higher crack-closure behavior. McEvily and Minakawa [13] have experimentally shown a rapid rise in the crack-closure behavior as the threshold is approached. Newman [14] has numerically shown that this behavior may be due to remote closure. Forth et al. [15], using a compression-compression pre-cracking constant-amplitude test procedure, has recently shown that fatigue-crack-growth thresholds are significantly lower, especially for low R ratios, than those reported in the literature, using the standard load-reduction procedure, on the 7075 plate material. Further study is needed to resolve this issue.

In Figure 1, the large open circles with the solid lines show the ΔK_{eff} -rate baseline relation chosen to fit these data and used as the table-lookup input, eqn (1), in the FASTRAN code. The upper solid curve shows a calculation of ΔK_{eff} -against-rate for one of the M(T) specimens ($w = 51 \text{ mm}$) to show how the calculated results are approaching fracture. The dashed lines show the results from a thin-sheet 7075-T6 alloy [12], which fell fairly close to the current results.

3.2 Titanium alloy – Ti-62222

The fatigue-crack growth results are shown in Figure 2. This figure shows Elber's effective-stress-intensity-factor, ΔK_{eff} , against crack-growth rate. The crack-opening stress equation [7] from the crack-closure model, FASTRAN, was used to correlate the data. The symbols show test results from the various laboratories. For crack-growth rates less than about $8\text{e-}4 \text{ mm/cycle}$, a constraint factor, α , of 2 was used and above a rate of about $8\text{e-}3 \text{ mm/cycle}$, a constraint factor, α , of 1.2 was used. The constraint-loss regime has been associated with the transition from flat-to-slant (45°) crack growth. The dotted vertical lines show the measured flat-to-slant transition from one of the M(T) specimens. This range also corresponds to the rapid change in rates measured on all specimens. Again, the crack-closure model correlated the fatigue-crack-growth rate data in a tight band. More scatter was observed in the constraint-loss regime, as the ESE(T) specimens grew to failure and in the near threshold regime. In the threshold regime, the results from Liknes and Stephens [9] at $R = 0.1$ and 0.5 were determined by using a load-reduction procedure. It has been shown that the load-reduction procedure may induce higher crack-closure behavior from tests [13] and from analyses [14] due to remote closure.

In Figure 2, the large open circles with the solid lines show the ΔK_{eff} -rate baseline relation chosen to fit these data and used as the table-lookup input, eqn (1), in the FASTRAN code. The dashed curve shows a calculation of ΔK_{eff} -against-rate for one of the M(T) specimens to show how the calculated results go to failure similar to the M(T) and ESE(T) specimens.

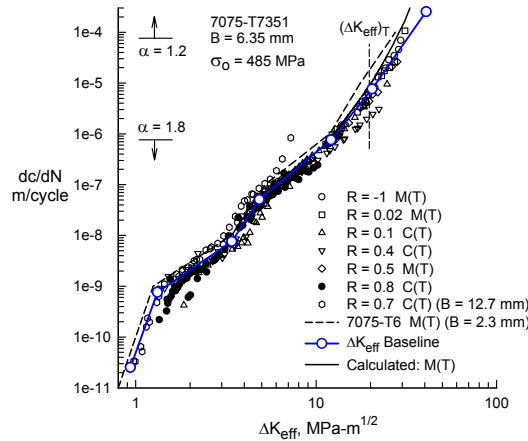


Figure 1: Effective stress-intensity factor against rate relation for the aluminum alloy.

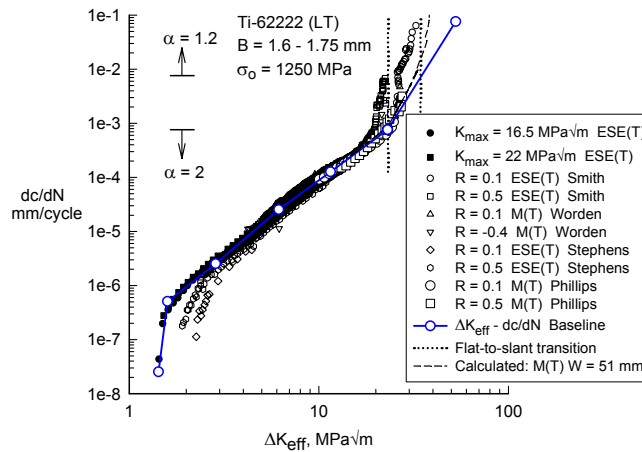


Figure 2: Effective stress-intensity factor against rate relation for the titanium alloy.

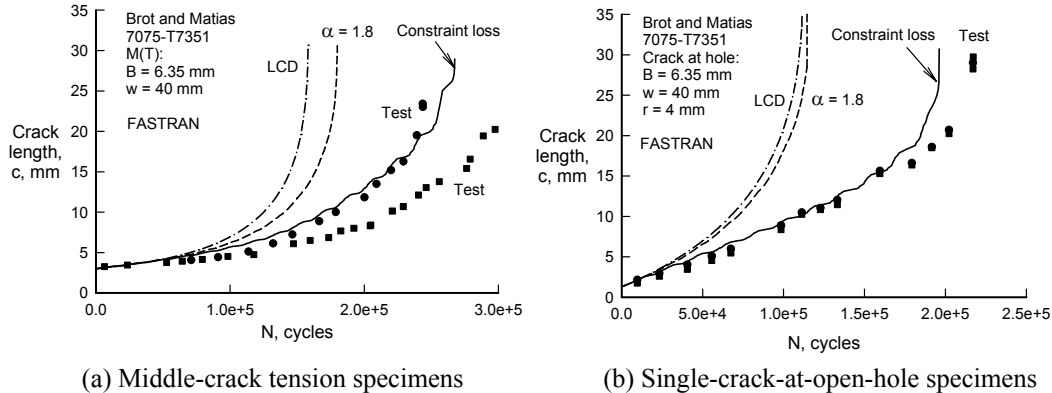
4 ALUMINUM ALLOY 7075-T7351

The details on the wing gust and maneuver spectrum are given in Reference 5. This spectrum simulates the gust and maneuver loading on a wing of a transport aircraft and is composed of seven levels of loading with a mean value of $R = 0.6$. The minimum stress in some flights will reach a compressive value of about 0.23 times the peak stress.

For the M(T) specimens subjected to the wing gust and maneuver spectrum, the two tests showed slightly different behavior, as shown in Figure 3(a). In the FASTRAN life-prediction code, the standard K-solution for the M(T) specimen was used. The linear-cumulative damage (LCD) and the constant constraint options ($\alpha = 1.8$) using FASTRAN produced nearly the same results. But the LCD calculations were roughly a factor-of-2 short of the test data, whereas, the constraint-loss option matched one of the tests quite accurately. The calculated results show regions of slow and rapid crack growth as the variable-amplitude loads are applied. This growth behavior is similar to what is seen in the second test. The FASTRAN prediction was within 20% of the average between the two tests at various crack lengths.

In Figure 3(b), two duplicate tests on the open-hole specimens produced almost exactly the same crack-length-against-cycles results. The stress-intensity factor solution used in FASTRAN

for this crack configuration is a friction-gripped specimen under remote uniform displacement with a specimen-height-to-width (h/w) ratio of 3. This case produced slightly lower, 0.1 to 9%, stress-intensity factors than remote uniform stress, when the crack length plus hole radius was between 0.5 and 0.85 of the width, respectively. However, the influence on life was not very significant. Again, the LCD and constant constraint results produced nearly the same crack-length-against-cycles results (a factor-of-2 short of the tests), but the constraint-loss option matched the test results until the specimen began to fail (within 10% at failure).



(a) Middle-crack tension specimens (b) Single-crack-at-open-hole specimens
Figure 3: Measured and predicted crack-length-against-cycles for under wing loading.

5 TITANIUM ALLOY TI-62222

The cyclic stress spectrum for a location on an HSCT lower wing surface was received from a major aircraft manufacturer and was transformed into a test load sequence [6]. Each flight was divided into seven flight segments (taxi out, climb, supersonic cruise, descent, subsonic cruise, approach, and taxi in). For testing purposes, it was decided to apply the spectrum as a repeated sequence of 1,600 flights (about 0.1 of a lifetime). The complete 1,600 flight load sequence contained 2,304,057 stress cycles. This was considered too long for testing, so a shorter test sequence was generated. The cyclic content of the test sequence is given in Reference 6.

For the HSCT spectrum, tests were conducted on M(T) specimens at three different maximum stress levels (207, 276 and 345 MPa). The test results are shown in Figure 6 at room temperature. Generally, only one test was conducted at each stress level, but two tests were conducted at the mid-stress level. The solid curves are the predicted results from FASTRAN using the baseline relation shown in Figure 2. The predicted results fell slightly short in cycles, but agreed very well with the test data (within 10%).

6 CONCLUSIONS

A “plasticity-induced” crack-closure model, FASTRAN, was used to correlate fatigue-crack-growth-rate data on 7075-T7351 aluminum alloy plate ($B = 6.35$ mm) and on a thin-sheet titanium alloy Ti-62222 STA alloy ($B = 1.6$ to 1.75 mm) under constant-amplitude loading over a wide range of stress ratios ($R = -1$ to 0.8 on the aluminum alloy and $R = -0.4$ to 0.5 on the titanium alloy). Crack-growth-rate data from near threshold to fracture were correlated, but the low R ratio data in the near threshold regime were neglected. Near threshold data generated with load-reduction procedures are suspected to generate inappropriately high thresholds because of remote closure due to load-history effects. Constraint factors, which account for three-dimensional state-of-stress effects in the crack-front region, were used in determining the effective-stress-intensity-factor-range-against-crack-growth-rate relation. Based on the spectrum crack-growth results, a constraint-loss regime was selected, which also roughly corresponds to the flat-to-slant crack-

growth region. Comparisons made between measured and calculated fatigue-crack-growth lives under the simulated aircraft load spectra agreed quite well (within 20 % of the test results).

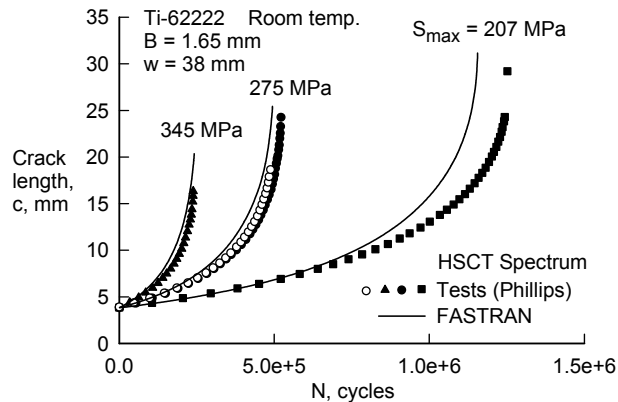


Figure 6: Measured and predicted crack-length-against-cycles for HSCT loading.

7 REFERENCES

1. Elber W. (1970) Fatigue crack closure under cyclic tension. *Engng Fract Mech*, 2:37-45.
2. Suresh S and Ritchie R. (1982) A geometric model for fatigue crack closure induced by fracture surface roughness. *Metallurgical Trans*, 13A:1627-1631.
3. NASGRO Reference Manual - Version 4.02. NASA Johnson Space Center and Southwest Research Institute, 2002.
4. AFGROW Reference Manual - Version 4.0. Wright-Patterson Air Force Base, AFRL/VASM, 2003.
5. Brot A and Matias C. (2002) An evaluation of several retardation models for crack growth prediction under spectrum loading. USAF Aircraft Structural Integrity Program Conference, Savannah, GA.
6. Phillips EP. (1999) Periodic overload and transport spectrum fatigue crack growth tests of Ti-62222STA and Al2024T3 sheet. NASA TM-208995.
7. Newman Jr JC. (1992) FASTRAN II - A fatigue crack growth structural analysis program. NASA TM-104159.
8. Smith S and Piascik R. (2000) An indirect technique for determining closure-free fatigue crack growth behavior. *ASTM STP 1372*:109-122.
9. Liknes H and Stephens R. (2000) Effect of geometry and load history on fatigue crack growth in Ti-62222. *ASTM STP 1372*:175-191.
10. Newman Jr JC. (1976) Fracture analysis of various cracked configurations in sheet and plate materials. *ASTM STP 605*:104-123.
11. Newman Jr JC. (1981) A crack-closure model for predicting fatigue crack growth under aircraft spectrum loading. *ASTM STP 748*:53-84.
12. Newman Jr JC. (1992) Effects of constraint on crack growth under aircraft spectrum loading. *Fatigue of Aircraft Materials*, Beukers et al, editors, Delft University Press, 83-109.
13. Minakawa K and McEvily AJ. (1981) On crack closure in the near threshold region. *Scripta Metallurgica* 15:633-636.
14. Newman Jr JC. (1983) A nonlinear fracture mechanics approach to the growth of small cracks. *Behaviour of Short Cracks in Airframe Materials*. AGARD CP 328:6.1-6.26.
15. Forth SC, Newman Jr JC and Forman RG. (2003) On generating fatigue crack growth thresholds. *Int J Fatigue*, 25:9-15.